A narrow-band injection-seeded pulsed titanium : sapphire oscillator-amplifier system with on-line chirp analysis for high-resolution spectroscopy

Hannemann, S.; van Duijn, E.J.; Ubachs, W.M.G.

published in
Review of Scientific Instruments
2007

DOI (link to publisher)
10.1063/1.2789690

document version
Publisher's PDF, also known as Version of record

A narrow-band injection-seeded pulsed titanium:sapphire oscillator-amplifier system with on-line chirp analysis for high-resolution spectroscopy

S. Hannemann, E.-J. van Duijn, and W. Ubachs
Laser Centre, Department of Physics and Astronomy, Vrije Universiteit, De Boelelaan 1081, 1081 HV Amsterdam, The Netherlands

(Received 31 May 2007; accepted 28 August 2007; published online 4 October 2007)

A narrow-band tunable injection-seeded pulsed titanium:sapphire laser system has been developed for application in high-resolution spectroscopic studies at the fundamental wavelengths in the near infrared as well as in the ultraviolet, deep ultraviolet, and extreme ultraviolet after upconversion. Special focus is on the quantitative assessment of the frequency characteristics of the oscillator-amplifier system on a pulse-to-pulse basis. Frequency offsets between continuous-wave seed light and the pulsed output are measured as well as linear chirps attributed mainly to mode pulling effects in the oscillator cavity. Operational conditions of the laser are found in which these offset and chirp effects are minimal. Absolute frequency calibration at the megahertz level of accuracy is demonstrated on various atomic and molecular resonance lines. © *2007 American Institute of Physics.* [DOI: 10.1063/1.2789690]

I. INTRODUCTION

Titanium:sapphire (Ti:sapphire, $Ti:Al_2O_3$) lasers share the advantages of broad wavelength coverage and tunability with the ease of use of an all-solid-state laser system. Besides continuous-wave lasing at ultranarrow bandwidths and employing the Kerr-lens mode-locking characteristic of the Ti:sapphire material to produce ultrashort laser pulses, pulsed lasing of Ti:sapphire in the nanosecond domain is a third often-used mode of operation. In applications where both narrow bandwidth and laser intensity are important, such as in non-linear spectroscopic applications as well as in LIDAR experiments, a nanosecond pulsed Ti:sapphire may be a system of choice.[1] In particular, satellite-based LIDAR systems benefit from the advantageous characteristics and the all-solid-state design of pulsed Ti:sapphire lasers.

In view of the fact that $Ti:Al_2O_3$ exhibits a rather long excited state lifetime of 3.15 μs,[2] the laser pulses generated in Ti:sapphire do not straightforwardly copy the pulse structure of typical *Q*-switched pump lasers, as is the case for dye lasers. Moreover, the broad gain profile requires careful wavelength selection, if the goal is narrow bandwidth single longitudinal mode (SLM) operation. In an early study by Brockman *et al.*,[3] both the pulse structure and wavelength selection were accomplished by injection seeding with the output of a pulsed dye laser. Injection seeding has remained a persistent theme in the design of narrow-band pulsed Ti:sapphire lasers. Georges *et al.*[4] have shown that in injection-seeded passive amplifiers, gain saturation in combination with an appropriate number of traversals through the medium, provides desired pulse durations down to 20 ns. Rhines and Moulton[5] demonstrated SLM operation of a pulsed Ti:sapphire resonator by injection seeding with the output of a cw Ti:sapphire laser, while Bair *et al.*[6] and Raymond and Smith[7] showed that the low seed power of a cw diode laser was sufficient to produce narrow-band 30 ns pulses.

In recent years, further developments of pulsed Ti:sapphire lasers have been pursued along various directions. Brandi *et al.*[8] have generated Fourier-transform (FT) limited laser pulses in excess of 200 mJ at durations of 300 ps. The high peak intensities delivered were upconverted in gaseous jets to produce FT-limited pulses at extreme ultraviolet (XUV) wavelengths as low as 40 nm.[9] Seiler *et al.* followed a different strategy also aiming at producing narrow-band XUV radiation. They preprogrammed pulse envelopes, in the range of durations between 10 ns and 1 μs, by acousto-optical modulator (AOM) intensity modulating the output of a cw Ti:sapphire laser and subsequently amplifying these in a series of multipass amplifiers; this led to XUV pulses at bandwidths as low as 55 MHz.[10] Dupré and Miller extended the development of injection-seeded pulsed Ti:sapphire lasers, focusing on methods to optimize cavity stabilization, to achieve pulse energies of 100 mJ at bandwidths as low as 12–30 MHz [full width at half maximum (FWHM)] for use in high-resolution spectroscopy.[11]

When using injection-seeded pulsed laser systems in high-resolution spectroscopic applications, either at the fundamental wavelength or at generated harmonics, effects of time-dependent gain in the amplifier will give rise to phase excursions deviating from the carrier wave. These result in a phenomenon known as chirp: time-dependent variations of the output frequency of the laser over the time period of the pulse. The chirp effects may cause a net offset between the carrier frequency and the time-averaged frequency of the pulse and result in problems with frequency calibration of the spectroscopic lines under study. Such calibration problems were already identified by Wieman and Hänsch in the early study of atomic hydrogen,[12] where dye lasers were

used. Chu and co-workers[13,14] addressed the chirp issues of dye amplifiers and their consequences for precise frequency calibration in relation to the spectroscopy of positronium. Eyler and co-workers[15,16] thereupon investigated the phase dynamics of dye amplifiers in further detail, while Reinhard *et al.*[17] and Eikema *et al.*[18] developed methods to compensate for chirp effects by manipulating the phase of the seed light via an electro-optic modulator before amplification.

While the chirp phenomenon in traveling wave dye amplifier originates in the time dependent gain in the lasing medium, solid-state oscillator laser cavities exhibit similar frequency excursions, although these have a different cause. Here, as a result of a change of refractive index in the gain material during gain buildup, the optical path length of the cavity changes during the creation of the population inversion. As a result, the frequency of the generated pulse does not coincide with the seed frequency to which the empty cavity is locked; this phenomenon is a frequency-pulling effect and may be associated with chirp during the pulse. Such phenomena have been studied in alexandrite lasers[19] as well as in optical parametric oscillator devices.[20,21]

In this paper, we describe the operation of a pulsed Ti:sapphire laser system consisting of an injection-seeded oscillator and a bow-tie amplifier. In the characterization, the frequency-pulling and chirp effects are measured and quantified, while methods to reduce these disturbing effects for high-resolution spectroscopic applications of the system are discussed as well.

II. DESIGN AND OPERATION OF THE LASER SYSTEM

A. The Ti:sapphire oscillator

The Ti:sapphire laser system consists of two main components: the oscillator cavity, in which nanosecond pulses are generated, and the amplifier, where the cavity output is further enhanced for subsequent efficient harmonic generation. The pulsed Ti:sapphire oscillator is built in the form of a stable ring cavity in which a Brewster-cut Ti:sapphire crystal of length of 1.57 cm and front area of 4×4 mm^2 is placed. The titanium-ion doping is chosen such that 90% of the pump light at 532 nm is absorbed over the length of the crystal. A schematic view of the setup is shown in Fig. 1. The cavity length of 40 cm corresponds to a longitudinal mode spacing of 750 MHz. The two mirrors close to the crystal are concave with identical radius of curvature $r=-0.5$ m. They have dichroic coatings, designed to transmit the pump light at a wavelength of 532 nm and to reflect the Ti:sapphire fluorescent light with $R=99.9\%$ efficiency. The remaining mirrors are both flat. One of them is a highly reflective mirror mounted on a piezoelectric actuator in order to control the cavity length using the Hänsch-Couillaud (HC) locking scheme.[22] The other one is an output coupling mirror with a typical reflectivity of $R_{oc}=90$ %. The finesse varies depending on the seeding wavelength and used mirror set and attains values between 20 and 35.

For pumping, the second harmonic light from an injection-seeded *Q*-switched Nd:YAG (yttrium aluminum garnet) laser operating at 10 Hz repetition rate (Quanta Ray GCR 3 by Spectra Physics) is used. It provides FT-limited

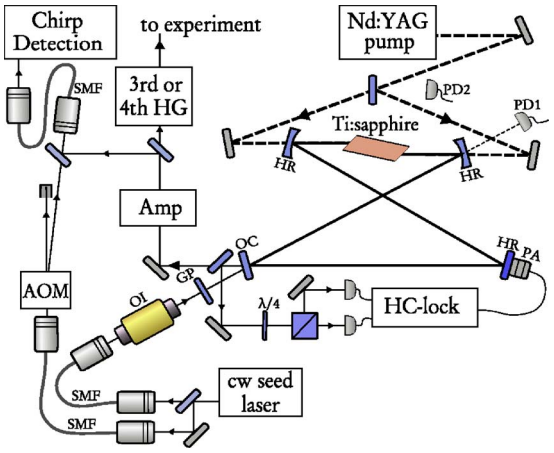

FIG. 1. (Color online) Schematic overview on the pulsed Ti:sapphire narrow-band oscillator. The cavity contains three high reflective (HR) mirrors, one output coupling (OC) mirror, and a Ti:sapphire crystal. One of the HR mirrors is mounted on a piezoactuator (PA), which is for maintaining the cavity length using the Hänsch-Couillaud (HC) locking scheme. For injection seeding light is coupled from a cw laser source through a single-mode fiber (SMF). The fiber tip is protected from pulsed amplification with an optical isolator (OI) and a glass plate (GP). The buildup process is monitored using two fast photodiodes: PD2 detects scattered pump light, and PD1 monitors cavity leak out. The amplifier (Amp) is depicted in Fig. 2.

pulses of 7 ns duration with a pulse timing root-mean-square (rms) jitter of 1.1 ns. From the maximum pulsed output of about 250 mJ at 532 nm, a fraction of 12 mJ is branched off for pumping the oscillator. The Ti:sapphire crystal is pumped from two sides in order to increase the maximum amount of pump energy possible to apply without exceeding the damage threshold of the Ti:sapphire crystal surface. The FWHM diameter $d_p=0.38$ mm of the intensity profile of the pump beam is matched to the cavity mode in the Ti:sapphire crystal.

Pumping the bare cavity without injection seeding produces broadband superfluorescence pulses in both directions. In order to obtain FT-limited pulses at a defined and controllable wavelength, the cavity is injection seeded using a few milliwatts of cw light from a Ti:sapphire ring laser (Coherent 899) or from an external cavity diode laser (Toptica DL 100) coupled through a single-mode polarization maintaining fiber. In order to protect the fiber tip from destructive effects of pulsed light traveling back to the aligned fiber, an optical isolator and a glass plate are placed between the fiber tip and cavity. The idea of the glass plate is the following: when aligned properly—at normal angle of incidence with the cavity mode—the amplified fluorescence propagating in the "wrong" direction toward the fiber tip is partially reflected ($R=4$ %) by the glass plate into the "right" direction. By this means, part of the gain into the wrong direction is transferred to the gain at the right direction, leading to an almost complete extinction of the amplification toward the fiber tip, while the pulse is formed. Thus, the glass plate ensures unidirectional pulse generation even for a nonseeded cavity providing additional safety for the fiber tip.

We did not investigate the operation of the system under different levels of seed power. We worked in a regime of sufficient seed power of about 30–50 mW from the cw Ti:sapphire laser or about 10 mW from the diode laser

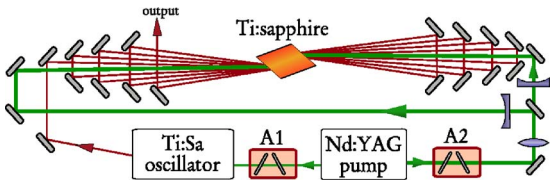

FIG. 2. (Color online) Schematic overview on the multipass amplifier system. The pump energies for both the oscillator and the amplifier can be varied between zero and full power using adjustable attenuators.

throughout this study. We note that the HC locking schemes operate on seed light reflected from the output coupler, thus setting a limitation on the power level.

B. The Ti:sapphire amplifier

Since the spatial cavity mode is rather narrow—with typical beam diameters of about 0.5 mm—the maximum output energy is restricted by the damage thresholds of the surfaces of the mirrors and the Ti:sapphire crystal. Pulse energies of up to 1 mJ can be generated from the Ti:sapphire oscillator. However, for reducing the probability of optical damage, typical output energies of 0.2–0.7 mJ are used. In order to enhance the pulse energies to about 10–40 mJ, an external multipath bow-tie shaped amplifier is available, which is schematically depicted in Fig. 2. It is pumped from two sides using the major part of the green output of the Nd:YAG laser which pumps the oscillator. The amplification can be varied using an adjustable pump light attenuator or by varying the number of amplification steps through the crystal.

C. Frequency upconversion

For most spectroscopic applications carried out with the Ti:sapphire laser system, harmonics of the near infrared output are used. In Fig. 3 the frequency upconversion setup as it has been used for the fourth harmonic is depicted. It involves second harmonic generation (SHG) using a β-Barium-Borate (BBO) cut at $\theta=30°$, subsequent frequency mixing of the second harmonic with the fundamental frequency light using a BBO $\theta=45°$, and finally mixing the third harmonic with the fundamental frequency provided by the remainder of the SHG stage in BBO $\theta=65°$.

All mixing stages use type-I phase matching, for which $\lambda/2$-retarder plates are placed to adjust the polarization planes of the second harmonic and of the third harmonic in front of the next upconversion step. The advantage of such a mixing scheme over a simpler double SHG scheme is its wide tunability range. While a double SHG system provides phase matching for $\lambda > 206$ nm, the mixing scheme over three upconversion stages extends the working range to $\lambda > 189$ nm limited by the absorption wavelength of BBO.

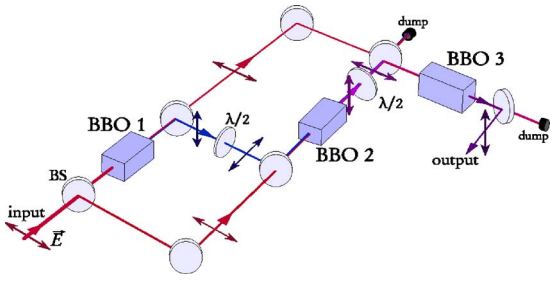

FIG. 3. (Color online) Schematic overview of the upconversion stages for the production of up to the fourth harmonic. The polarization planes are indicated with arrowed lines. All phase matching is of type I. $\lambda/2$-retardation plates turn the polarization to the desired plane.

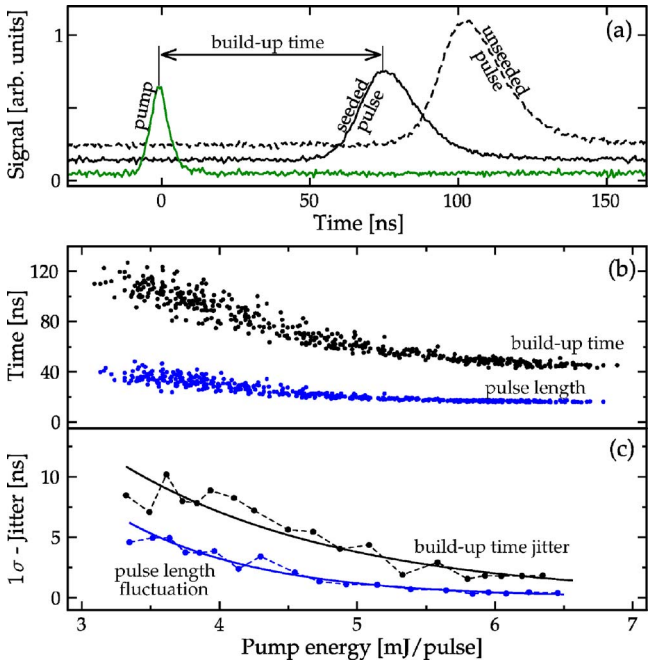

FIG. 4. (Color online) Pulse generation dynamics of the Ti:sapphire oscillator cavity. (a) Oscilloscope traces of a pulse buildup process inside the cavity registered for one single injection-seeded pulse event and one without the seeding. (b) Buildup time and pulse length as depending on the pump energy. (c) Statistical fluctuations given as local standard deviations (from 25 shots per measurement) of the buildup time and the pulse duration decrease with rising pump energy.

The achieved upconversion efficiencies are 50% after the near infrared for the SHG, 30% of the SHG for the third harmonic, and finally about 10% of the third harmonic for the fourth harmonic. The maximum output energies obtained at 212–196 nm were 0.1–0.3 mJ. For the double SHG stage system, larger output energies are achieved since it involves only two nonlinear conversion stages. For infrared output energies of about 16 mJ, output energies of 2 mJ were reached at $\lambda=212$ nm.

III. LASER CHARACTERISTICS

A. Pulse buildup time and pulse length

First of all, the lasing dynamics of the cavity determining both the time delay between the pump pulse arrival and infrared pulse generation and the pulse duration are investigated. In Fig. 4, oscilloscope traces of a typical pulse timing sequence are shown. The response time of the photodetection system is estimated to be about 1 ns. The timing difference between peak intensities of pump and output pulses is defined as the pulse buildup time. The unseeded buildup process takes somewhat longer than the injection-seeded process, an observation found to be consistent throughout the entire wavelength range (764–856 nm) over which the seeding light was tuned.

The dynamics of the buildup process is strongly affected by the pulse energy of the pump laser because it determines the population inversion and thereby the initial gain in the active laser medium. As the lifetime of the excited state in Ti:sapphire is 3.15 μs,[2] the pulse amplification continues over several cavity round trip times until the population inversion is depleted by the amplification process. At the level where laser gain and cavity loss are equal, the infrared pulse intensity reaches its maximum; thereafter, the gain decreases further and the pulse intensity drops to zero. In the example of Fig. 4, the seeded buildup process takes about 70 ns or, correspondingly, 53 cavity round trips.

In Fig. 4, also the observed buildup times, pulse lengths, timing jitter, as well as pulse length fluctuations are displayed as a function of pump pulse energy in the range of 2–7 mJ. It is apparent that the pulse production process becomes faster for higher pump pulse energies and that the pump pulse is sufficiently short to induce exactly one output pulse, while the buildup time is about an order of magnitude larger than the pump pulse duration. An advantage of the Ti:sapphire oscillator is that pulses of long duration can be generated because of the long storage time in this gain material, where the pulse length is determined by the balance between the gain and cavity loss. This in turn reduces the achievable Fourier-limited bandwidth in comparison with dye lasers where the pulse length is determined by the pump pulse duration. The lower part (c) of the figure shows locally calculated standard deviations of the buildup time and the pulse duration taken from 25 pulses each. Apparently, the pulse timing jitter of the oscillator is stronger for lower pump energies, i.e. closer to laser threshold. Since the pulse timing strongly depends on the pump power, it is a natural consequence of the power fluctuations of the Nd:YAG pump laser, which exhibit rms shot-to-shot energy fluctuations of 4.4%, that the generated pulses show timing jitter.

B. Conversion efficiency

The conversion efficiency of the Ti:sapphire oscillator was investigated in the range of 764–856 nm, covered by three mirror sets: a long wave set (LW) for 856–840 nm and two configurations for middle wave (MW) (806–806 nm) and short wave (SW) (813–764 nm). While for the MW and SW sets only the output coupling mirror is different, the LW mirrors form a completely different set. At each wavelength setting, the pump energy was varied and about 300–500 shots were acquired. The result of these conversion efficiency measurements is shown in Fig. 5. For each data set, a polynomial regression (third order) is performed and depicted as a solid line. The data points shown in the figure are averaged over 25 shots and connected with a dashed line.

The most significant result is that the SW mirror set provides a superior conversion efficiency over the other two mirror sets. The main difference between the SW and LW/MW mirror sets is the reflectivity of the output coupling mirror. The SW output coupler has a reflectivity of R=95% and the other two of about 88%. Correspondingly, the pump energies at which the oscillator reaches laser threshold are smaller for the SW mirrors than for the other sets. The conversion efficiency varies between 5% and 10%. As will be shown below, the HC-cavity lock setting not only affects the conversion efficiency but also controls any frequency deviation between the cw seed and the pulsed output. It was found that the highest conversion is achieved when the frequency deviation equals zero.

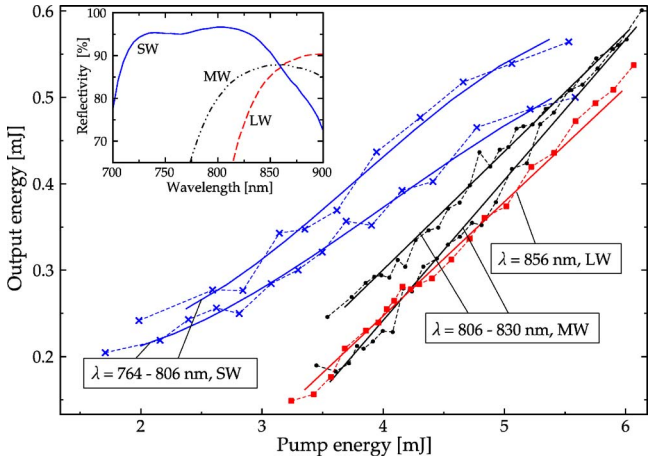

FIG. 5. (Color online) Energy conversion in the Ti:sapphire oscillator for different wavelengths using three different mirror sets (SW, MW, and LW). The reflectivities of the output coupling mirrors are shown in the inset.

C. Frequency evolution

The setup for a quantitative assessment of the instantaneous frequency excursions in the pulsed output is included in Fig. 1. Part of the seeding light is first shifted in frequency using an AOM and then heterodyned with the pulsed output of the oscillator. The generated beat pattern is detected using a fast photodiode and a fast oscilloscope (Tektronix TDS 7440, 4 GHz, 20 Gsamples/s). Any beatnote deviations from the AOM frequency (ν_{AOM}=250 MHz; the rf driver frequency is constant within 0.1 MHz and has neglibible drift) will be attributed to instantaneous frequency shifts between pulsed output and cw seeding light. The chirp analysis is performed on-line, during all following measurements.

In Fig. 6, the process of the Fourier analysis is schematically presented. In the upper part (a), a typical beat pattern is shown. First, the signal is Fourier transformed. In the power spectrum—depicted in Fig. 6(b)—one recognizes two characteristic peaks. The low frequency part results from the pulse envelope, while the frequencies around 250 MHz arise from the beatnote wiggle. As shown, the two components are well separated in frequency space. For two reasons, simple box shaped filters were applied. First, the spectral content in between the two main frequency components is several orders of magnitude weaker than that at the peaks. Second numerical efficiency is important in an on-line chirp analysis. The resulting subsets of the Fourier-transformed data are reversely Fourier transformed, yielding a noise reduced pulse envelope $\varepsilon(t)$ and the phase evolution $\Phi(t)$ of the beatnote wiggle. The time derivative of the phase evolution $\Phi(t)$ gives the instantaneous frequency of the beatnote wiggle, from which the AOM frequency ν_{AOM} is subtracted in order to obtain the temporal evolution of the pulsed-cw frequency offset,

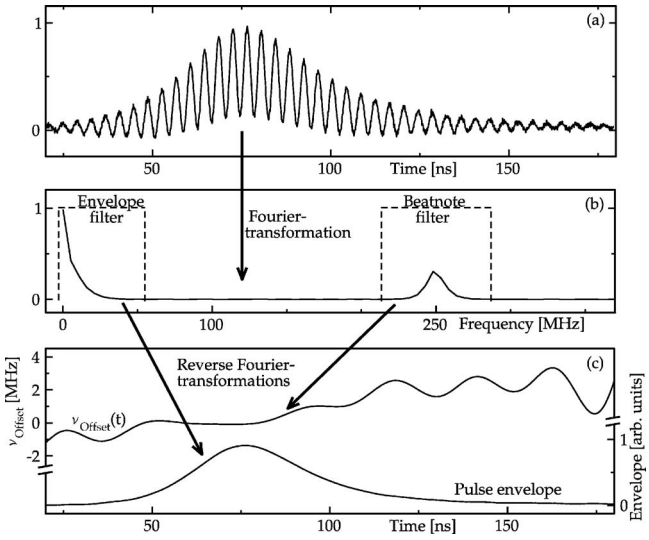

FIG. 6. Overview on the steps of the chirp analysis procedure. (a) The beat pattern between frequency shifted seeding light and the pulsed output of the cavity recorded on a fast photodiode and a fast oscilloscope. (b) The power spectrum showing the two main frequency components from the pulse envelope and from the beatnote. (c) Applying the frequency filters as sketched and reverse Fourier transformation yields the envelope and the instantaneous frequency of the pulse.

$$\nu_{\mathrm{offs}}(t) = \frac{1}{2\pi}\frac{d\Phi}{dt} - \nu_{\mathrm{AOM}}. \tag{1}$$

Examples of both the noise reduced envelope $\varepsilon(t)$ and the frequency offset are depicted in Fig. 6(c). The resulting instantaneous frequency offset can be approximated by a net frequency shift $\bar{\nu}_{\mathrm{offs}}$ and a linear frequency change in time $\tilde{\nu}_{\mathrm{lin}}$, which will be referred to as the linear chirp. In the following, focus is on how $\bar{\nu}_{\mathrm{offs}}$ and $\tilde{\nu}_{\mathrm{lin}}$ are affected by the pump energy, the seeding wavelength, and the HC-lock settings.

In order to calculate the net frequency offset $\bar{\nu}_{\mathrm{offs}}$, a weighted average on $\nu_{\mathrm{offs}}(t)$ is performed,

$$\bar{\nu}_{\mathrm{offs}} = \int \nu_{\mathrm{offs}}(t)w(t)dt, \quad w(t) = \frac{\varepsilon(t)}{\int \varepsilon(t)dt}, \tag{2}$$

where $w(t)$ is the normalized noise-filtered pulse envelope $\varepsilon(t)$. The linear frequency chirp $\tilde{\nu}_{\mathrm{lin}}$ is extracted from the instantaneous frequency evolution $\nu_{\mathrm{offs}}(t)$ by a weighted linear regression using the same weight function $w(t)$. A linear approximation $\tilde{\nu}_{\mathrm{offs}}(t)$ of the instantaneous pulsed-cw frequency offset $\nu_{\mathrm{offs}}(t)$ is written as

$$\tilde{\nu}_{\mathrm{offs}}(t) = \tilde{\nu}_0 + \tilde{\nu}_{\mathrm{lin}}t. \tag{3}$$

The parameters $\tilde{\nu}_0$ and $\tilde{\nu}_{\mathrm{lin}}$ are extracted using a weighted linear regression. It should be noted that in general $\tilde{\nu}_0$ is different from the net frequency shift $\bar{\nu}_{\mathrm{offs}}$.

Experimentally, it is important to know the net frequency shift $\bar{\nu}_{\mathrm{offs}}$ precisely and take it into account for an absolute frequency calibration. In Fig. 7, the frequency offset $\bar{\nu}_{\mathrm{offs}}$ and the linear frequency chirp $\tilde{\nu}_{\mathrm{lin}}$ are measured and analyzed via Eqs. (1)–(3) as a function of the pump energy at a fixed wavelength of $\lambda = 810$ nm. From the figure, one can see that the averaged offset frequency $\bar{\nu}_{\mathrm{offs}}$ decreases with rising pump energies. At low pump energies, the linear chirp rises slightly with increasing pump energies and obtains increasingly negative values for larger pump powers.

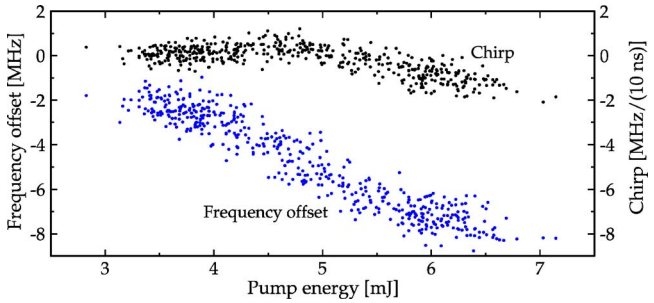

FIG. 7. (Color online) Typical behavior of the frequency offset $\bar{\nu}_{\mathrm{offs}}$ and the linear chirp $\tilde{\nu}_{\mathrm{lin}}$ of the pulsed output of the oscillator at a fixed wavelength $\lambda = 810$ nm and fixed HC setting for varying pump pulse energies. The linear chirp contribution starts around 0 MHz/(10 ns), rises slightly at low energies, and eventually becomes increasingly negative for larger pump energies. At the same time, the net pulsed-cw frequency shift $\bar{\nu}_{\mathrm{offs}}$ becomes more negative for higher pump energies.

D. Cavity mode pulling

In Fig. 8, the longitudinal cavity mode structure and the HC error signal are shown as functions of the seed light frequency. For optimal coupling of the seeding light into the cavity, the electronics has to be set such that the cavity is in perfect resonance with the frequency of the seeding light. This setting is labeled as "2" in Fig. 8. Since the buildup time in the pulsed oscillator is about three times longer than the actual pulse duration, the center frequency of the pulsed output will be strongly affected by the cavity mode structure. Such an effect, referred to as the "cavity mode pulling," has been observed before in other laser materials.[23,24] Also in a theoretical model by Bowers and Moody,[25] it is predicted that the output of injection-seeded pulsed laser systems, where the cavity round trip time is much shorter than the actual buildup time, the longitudinal mode structure of the cavity rather than the seed frequency, determines the center frequency of the output pulses. The seed frequency merely selects the cavity resonance frequency at which the output is pulled to. As a consequence, any deviation of the HC lock from ideal setting 2 will lead to frequency offsets between seeding light and pulsed output.

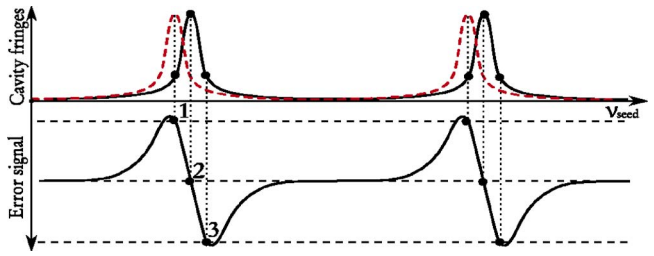

FIG. 8. (Color online) The Hänsch-Couillaud locking scheme. The error signal and the cavity fringes vs the seed frequency ν_{seed} are depicted. The thin dashed lines show three different voltage offset settings and the resulting lock point position relative to the cavity mode structure. The second and slightly displaced fringe pattern depicted as a (red) dashed line illustrates the fringe positions upon pumping the cavity.

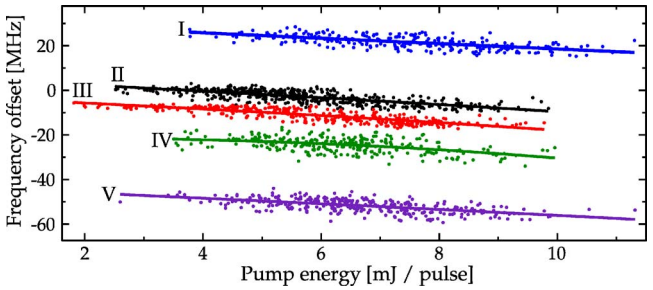

FIG. 9. (Color online) Set of measurements of the pulsed-cw frequency offset $\bar{\nu}_{\text{offs}}$ at $\lambda = 810$ nm and at different HC settings. With rising pump energies, $\bar{\nu}_{\text{offs}}$ becomes more negative. Using different HC settings (numbered from I to V), it is possible to tune the net frequency shift $\bar{\nu}_{\text{offs}}$ within a range between −50 and 25 MHz.

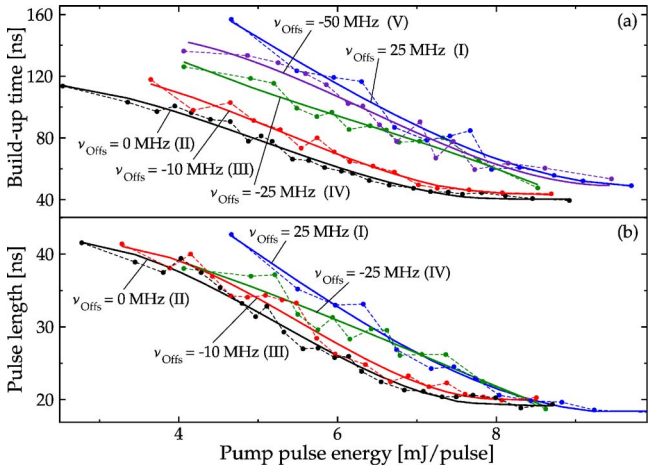

FIG. 10. (Color online) Buildup times and pulse durations measured at different HC-lock settings and varying pump energies. Numbering and color coding are consistent with Fig. 9. The trace for the pulse durations for a −50 MHz frequency offset setting (V) is not depicted in aid of a better view—it is located in the vicinity of settings I and IV.

However, this is valid for the nonpumped cavity only. When the pump pulse arrives, the refractive index of the Ti:sapphire crystal[26] and therewith the optical path length of the cavity are changed on a nanosecond time scale, which is instantaneous for the cavity mechanics. As a result of this optically induced refractive index change, the cavity resonances are shifted by a certain amount depending on the pump intensity and of the wavelength of the seeding light. In Fig. 8, the shifted cavity resonance pattern is depicted with a (red) dashed line.

To investigate the cavity mode pulling mechanism, a series of measurements has been performed at a fixed wavelength $\lambda = 810$ nm. For different HC settings, the pulsed-cw frequency offset $\bar{\nu}_{\text{offs}}$ is measured as a function of the pump pulse energy; results are depicted in Fig. 9. It shows that the pulsed-cw frequency offset strongly depends on the HC setting and to a lesser extent on the pump energy. For all tested HC-lock settings, the pulsed-cw offset $\bar{\nu}_{\text{offs}}$ is increasingly negative for increasing pump energies. An important practical conclusion from this measurement is that the HC lock can always be set such that $\bar{\nu}_{\text{offs}}$ is about zero. The range of pulsed-cw frequency offsets accessible by tuning the HC-lock point is related to the finesse of the oscillator cavity because that determines the width of the HC error signal. Note that the Roman numerals (I–V) in Fig. 9 and in figures introduced below refer to the same HC-lock settings.

Since the HC setting and the applied pump energy both affect the cavity length, the influence of the HC lock on the buildup timing, the pulse length, and the linear chirp is further investigated. In Fig. 10, the pulse buildup times and pulse durations are plotted for different HC-lock settings and varying pump energies. Indeed, the buildup times are shorter for HC settings, which produce small pulsed-cw frequency offsets and become longer for larger offsets. This can be explained by the influence of the longitudinal mode structure on the amplification gain. When the seeding light is in exact resonance with a specific mode of the pumped cavity, the injection-seeded amplification is most efficient as consecutive round trips are perfectly in phase. Slight phase mismatches are disadvantageous for the amplification. Eventually, the center frequency in the pulse amplification is pulled toward the cavity resonance even when it starts with a considerable frequency mismatch between the seed and cavity resonance. Thus, the buildup time is shortest for a zero frequency offset setting of the HC lock; this phenomenon could possibly be used in an improved cavity locking scheme.

In Fig. 11, the results for the measurements of the linear chirp $\tilde{\nu}_{\text{lin}}$ are shown. The five traces for the different HC settings denoted with the corresponding pulsed-cw frequency offset have in common that for higher pump energies, the chirp becomes increasingly negative. However, for HC settings with low pulsed-cw frequency offsets, the linear chirps change more drastically for increasing pump power.

E. Wavelength dependence of the frequency excursions

As was shown, the HC settings can be used to tune the pulsed-cw offset $\bar{\nu}_{\text{offs}}$ to zero. This setting, coinciding with short buildup times and pulse lengths at a given seeding wavelength and pump energy, was chosen in the following measurements. In Fig. 12, the buildup timing and pulse durations are plotted for different wavelengths and different mirror sets. Conditions of wavelengths and mirror sets delivering the largest amplification gain per cavity round trip are expected to provide the shortest buildup times. In part (a) of the figure, the buildup times for the SW mirror set are the shortest. This is a result of cavity losses with the SW mirrors being a factor of 2 smaller than for the other sets.

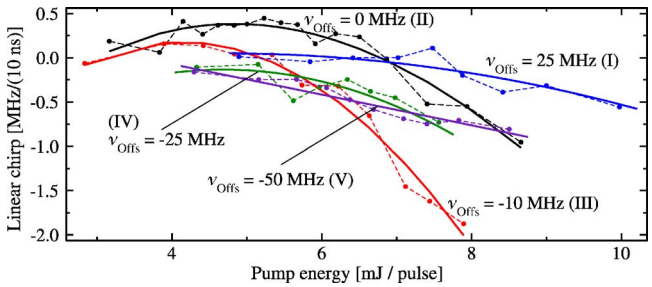

FIG. 11. (Color online) Experimental data for the linear frequency chirp $\tilde{\nu}_{\text{lin}}$ measured at $\lambda = 810$ nm and different HC settings at varying pump energies. For higher pump energies, the linear chirp becomes increasingly negative.

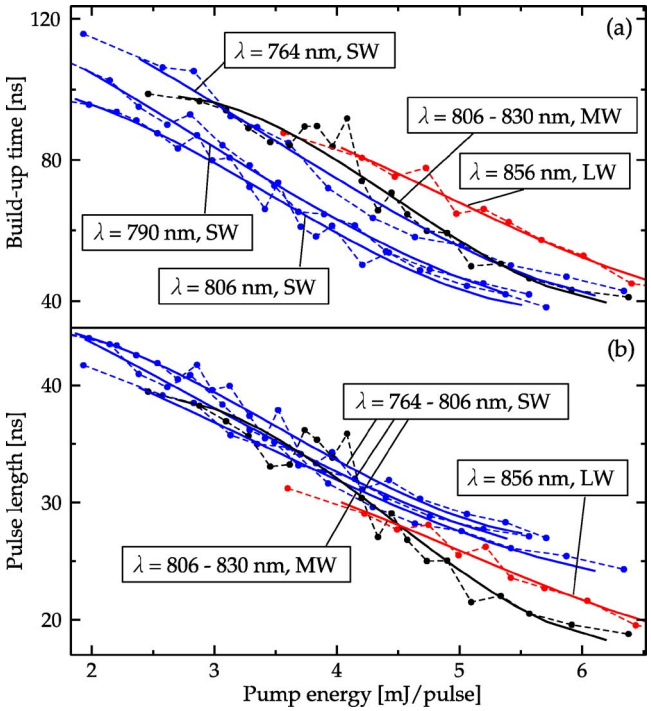

FIG. 12. (Color online) Wavelength dependence of the (a) buildup time and (b) pulse duration at zero pulsed-cw frequency offset and varying pump energies. Labels indicate additionally the used mirror set (cf. inset in Fig. 5).

Next to the lasing dynamics, an important question is how the linear chirp depends on the wavelength. To investigate this, the linear chirp $\tilde{\upsilon}_{\mathrm{lin}}$ was measured as a function of the pump energy at different seed wavelengths, still retaining zero frequency offset conditions. In Fig. 13, the measured linear chirp values are shown. The linear chirps attain values close to zero for wavelengths in the vicinity of 800 nm, where even for increased pump energies the pulses maintain their low chirp characteristic. For shorter wavelengths, the linear chirp becomes increasingly positive and for longer wavelengths increasingly negative. The linear chirp becomes generally stronger for higher pump energies.

The results in Figs. 7 and 9 show that the pulsed-cw frequency offset $\bar{\nu}_{\mathrm{offs}}$ varies with the applied pump energy.

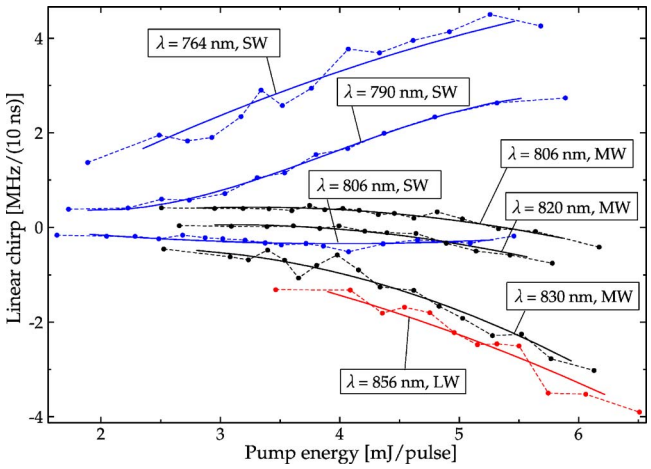

FIG. 13. (Color online) Linear chirp $\tilde{\nu}_{\mathrm{lin}}$ measured at different wavelengths, zero pulsed-cw frequency offset, and varying pump energy.

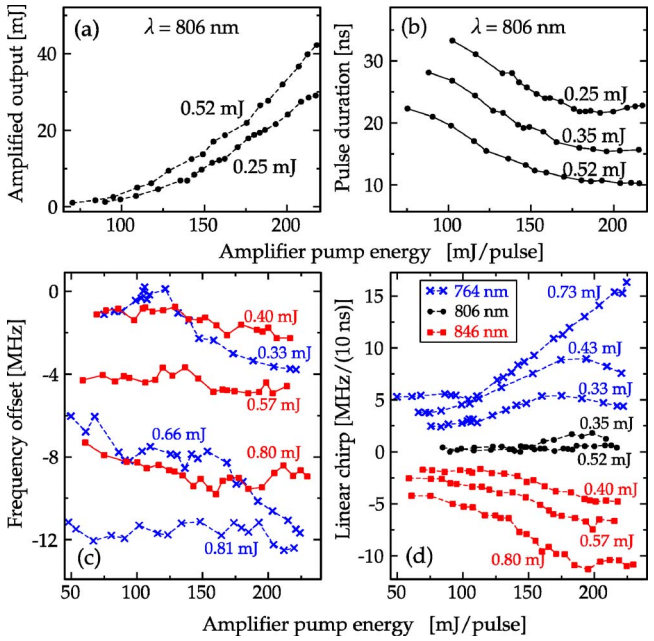

FIG. 14. (Color online) Effect of the external amplification on several characteristics of the pulsed output of the oscillator: (a) pulse energy, (b) pulse duration, (c) pulsed-cw frequency offset $\bar{\nu}_{\mathrm{off}}$ (see text), and (d) linear chirp $\tilde{\nu}_{\mathrm{lin}}$. The pulse energies indicated as data labels represent the values before amplification.

The reason for this behavior is an optically induced refractive index change Δn in the Ti:sapphire crystal, which depends on the applied pump energy and affects the longitudinal mode structure of the cavity. Since the buildup time is much longer than the round trip time of the cavity and the amplification from the seed light intensity level to the maximum pulsed intensity exceeds four orders of magnitude, the pulsed output frequency ν_{out} will be completely pulled from the seed frequency ν_{cw} to the closest pumped cavity resonance position ν_p. We have performed a numerical analysis linking the frequency offsets $\bar{\nu}_{\mathrm{offs}}$ as a function of pump fluence in the Ti:sapphire oscillator to changes Δn in the refractive index in the gain material. Here we restrain ourselves to the phenomenology of the laser operation and refer for details on the numerical analysis to Ref. 27.

F. Amplifier effects

For the investigation on how the pulse characteristics are affected by the external amplification, systematic measurements are performed on the pulse duration, the pulse energy, the mean pulsed-cw frequency offset $\bar{\nu}_{\mathrm{offs}}$, and the linear chirp $\tilde{\nu}_{\mathrm{lin}}$. Three different seeding wavelengths were chosen at which all of the listed characteristics are measured: one at wavelength (806 nm) close to the top of the Ti:sapphire gain profile, one at the long wavelength (846 nm) side, and on at the short wavelength (764 nm) side of the range of operation of the laser. For all measurements, the external amplification comprises eight passes through the Ti:sapphire crystal. Results are depicted in Fig. 14.

For the pulse duration and pulse output energies, the obtained results are rather similar and do not depend on the wavelengths. Therefore, in Figs. 14(a) and 14(b), only results for $\lambda = 806$ nm are represented. The output energy increases

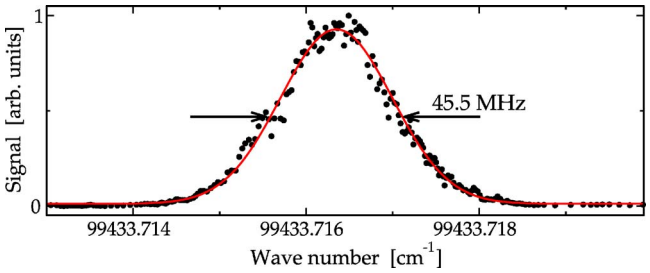

FIG. 15. (Color online) The $Q(1)$ line of the EF$\leftarrow X$ (0,0) band in D_2 measured in a 2+1 REMPI process with the FWHM of 45.5 MHz is indicated.

with the pump energy applied to the Ti:sapphire crystal and with the oscillator output energy. A maximum of 41 mJ amplified output is achieved, corresponding to a conversion efficiency of 18%. Apparently, the pulse duration is shortened for strong external amplification. At the setting at which the oscillator produces 0.25 mJ in a pulse duration of about 35 ns, the amplified output is shortened to 22 ns at maximum amplification.

In Fig. 14(c), the results for the measurements of the mean pulsed-cw frequency offset $\bar{\nu}_{\mathrm{offs}}$ of the amplified output are shown. Here, the results for wavelengths of 764 and 846 nm are displayed. The results at $\lambda=806$ nm are similar to these. Apparently, the amplification changes $\bar{\nu}_{\mathrm{offs}}$ by maximally 5 MHz at a wavelength of 764 nm for the medium cavity pump setting at which the oscillator output was 0.66 mJ.

Results on the linear chirp $\tilde{\nu}_{\mathrm{lin}}$ in the traveling wave amplification process at three wavelengths are depicted in Fig. 14(d). This shows that the linear chirp becomes more pronounced by the amplifier. For the short wavelength (764 nm), the linear chirp is positive and increases for higher oscillator output energies and increasing amplifier pump energies, while at the long wavelength (846 nm) the chirp is negative and becomes more negative under conditions of more intense pumping. At a wavelength of 806 nm, the linear chirp remains in the vicinity of zero during external amplification. Without going into a physical interpretation of chirp effects in the amplifier, we just note that here frequency pulling (as in the oscillator) cannot be the underlying mechanism and that most likely phase modulation is at the origin of the observed process.

G. Laser bandwidth

For application in laser spectroscopic experiments, the spectral bandwidth of a laser source is a crucial parameter. Here the bandwidth is derived from the measurement of a spectral line shape under conditions at which the profile is fully determined by the laser bandwidth properties. The $Q(1)$ line in the EF-X (0,0) band in the D_2 molecule is probed via 2+1 resonance enhanced multiphoton ionization using a wavelength near $\lambda=202$ nm. The spectrum is displayed in Fig. 15.

The measurement conditions entail (i) two-photon excitation with counterpropagating beams, thus imposing Doppler-free circumstances; (ii) collision-free conditions of a molecular beam, therewith avoiding collisional broadening; (iii) excitation with low laser intensity to ensure that the ac Stark effect broadening is below 1 MHz; and (iv) an excited state lifetime of about 200 ns,[28] causing lifetime broadening below 1 MHz. Under these conditions, the spectral line profile, represented by a Gaussian with a width of $\Delta\nu=45.5$ MHz, is entirely determined by the spectral bandwidth properties of the laser at its fourth harmonic. Taking into account the two-photon excitation and fourth harmonic generation and assuming a Gaussian frequency profile, the spectral output of the Ti:sapphire laser can be derived at $\Delta\nu_{\mathrm{IR}}=16$ MHz.

During the spectroscopy on the D_2 line, the following laser settings were used. To generate chirp reduced pulses at reasonably stable lasing conditions, the oscillator pump was adjusted such that the pulse buildup time in the oscillator was consistently maintained at 80 ns. The amplifier output was adjusted to 8 mJ. Using the MW mirror set, the oscillator produced pulses of 0.3 mJ energy and 30 ns duration. The amplifier shortened the pulses to about 25(3) ns, which corresponds to a Fourier-transform-limited spectral width of 17.5(2.5) MHz for ideally Gaussian shaped pulses, which is in agreement with the estimated value of 16 MHz derived from the spectral measurement shown in Fig. 15.

IV. SPECTROSCOPIC APPLICATIONS OF THE Ti:SAPPHIRE SOURCE IN THE DEEP ULTRAVIOLET

The combination of the pulsed mode of operation providing high peak intensities with the Fourier-transform-limited spectral properties, this Ti:sapphire laser system, is suitable for the nonlinear frequency upconversion. The control over the frequency evolution during the laser pulses makes it a versatile instrument for high precision spectroscopies in the deep UV, as an alternative to a chirp-controlled optical parametric oscillator.[29] Various spectroscopic investigations have been performed employing, in particular, the fourth harmonic at about 200 nm of the output pulses. In the spectroscopic studies, the on-line chirp analysis was performed to extract $\bar{\nu}_{\mathrm{offs}}$ and the transition frequencies of the resonances at the highest level of accuracy. Frequency calibration was derived from calibration of the seed laser against a frequency comb laser as described in Ref. 30 In addition, the laser excitation of atoms and molecules in a crossed-beam configuration was performed with counterpropagating laser beams in a geometry of Sagnac interferometer to reduce Doppler shifts.[31]

In one-photon laser-induced-fluorescence atomic beam studies, the transition frequency of the singlet $3s\rightarrow 4p$ resonance in Mg at $\lambda=202$ nm was investigated, yielding a transition frequency at an accuracy of ≈ 1 MHz.[32] Also the $3s\rightarrow 3p$ resonance in Mg at $\lambda=285$ nm was calibrated to the megahertz level of accuracy using the third harmonic ultraviolet output.[33] Several two-photon excitation frequency metrologies were performed as well: on the EF$\leftarrow X$ transition in molecular hydrogen and some of its isotopomers[30] and on the $4p^6\rightarrow 4p5p[1/2]_0$ transition in krypton, both yielding accuracies at the megahertz level. In addition, this krypton transition was employed in a resonance enhanced sum-frequency mixing scheme, for efficient upconversion of the

narrow-band output at $\lambda = 212$ nm to the XUV range near 90 nm; at these wavelengths, high-resolution spectroscopy was performed on narrow resonances in the H_2 and N_2 molecules.[34] In this resonance enhanced sum-frequency mixing experiment, a cw laser diode operating at wavelengths about 850 nm was implemented,[34] showing that a system of diode lasers, covering the wavelength range of Ti:sapphire lasers, can be used alternatively as seed light source.

Furthermore, the laser system was employed in a demonstration experiment where cavity ringdown spectroscopy at the shortest wavelengths so far—down to 197 nm—was performed.[35] Spectral lines in the lowest (0,0) Schuman-Runge band of molecular oxygen were investigated in more detail (also near $\lambda = 202$ nm), both by laser-induced-fluorescence and cavity ringdown methods.[36] The ultranarrow bandwidth in the deep-UV region allowed for a determination of the pressure shift as well as of the predissociation rate of single resolved fine-structure states in the $B\,^3\Sigma_u^-$, $v=0$ state of the molecule. These studies amply demonstrate the versatility of the Ti:sapphire laser system for high-resolution spectroscopic applications.

V. CONCLUSION

The perspective of the present investigation and analysis of the characteristics of the laser system is aimed at precision calibration application in high-resolution spectroscopy, rather than obtaining a full physical understanding of the processes occurring in the laser. Next to the lasing dynamics which include the pulse buildup time, pulse duration, and conversion efficiency, special emphasis was put on the frequency evolution of the generated pulses because that usually is the limiting factor in the accurate determination of the transition frequency of a spectral feature.

We note that, although the quantitative chirp phenomena are similar in effect, the underlying physical mechanisms in the Ti:sapphire oscillator are different from traveling wave optical systems as the external Ti:sapphire amplifier or pulsed dye amplifiers. The performed measurements revealed the influence of the mode structure of the oscillator cavity on the pulses ("cavity mode pulling"), most notably on the net pulsed-cw frequency offset.

The presented chirp analysis is implemented as a single-shot technique allowing to monitor frequency differences between seed light and pulsed output at real time. The cavity mode pulling can be "tuned" using the Hänsch-Couillaud lock yielding zero pulsed-cw frequency offsets. The chirp effects depending on the seed wavelength and the pump intensity are less controllable: working with low pump intensities is the most efficient, but not always an available option to minimize the chirp. The wide wavelength range of Ti:sapphire, the narrow-band pulsed characteristics, accurate frequency control, and referencing techniques make this laser a flexible instrument for high precision metrology in the deep ultraviolet.

ACKNOWLEDGMENTS

The Netherlands Foundation for Fundamental Research on Matter (FOM) is gratefully acknowledged for financial support.

[1] K. Ertel, H. Linné, and J. Bösenberg, Appl. Opt. **44**, 5120 (2005).
[2] P. Moulton, J. Opt. Soc. Am. B **3**, 125 (1986).
[3] P. Brockman, C. H. Bair, J. C. Barnes, R. V. Hess, and E. V. Browell, Opt. Lett. **11**, 712 (1986).
[4] P. Georges, F. Estable, F. Salin, J. P. Poizat, P. Grangier, and A. Brun, Opt. Lett. **16**, 144 (1991).
[5] G. A. Rhines and P. Moulton, Opt. Lett. **15**, 434 (1990).
[6] C. H. Bair, P. Brockman, R. V. Hess, and E. A. Modlin, IEEE J. Quantum Electron. **24**, 1045 (1988).
[7] T. D. Raymond and A. V. Smith, Opt. Lett. **16**, 33 (1991).
[8] F. Brandi, I. Velchev, D. Neshev, W. Hogervorst, and W. Ubachs, Rev. Sci. Instrum. **74**, 32 (2003).
[9] F. Brandi, D. Neshev, and W. Ubachs, Phys. Rev. Lett. **91**, 163901 (2003).
[10] R. Seiler, Th. Paul, M. Andrist, and F. Merkt, Rev. Sci. Instrum. **76**, 103103 (2005).
[11] P. Dupré and T. A. Miller, Rev. Sci. Instrum. **78**, 033102 (2007).
[12] C. Wieman and T. W. Hänsch, Phys. Rev. A **22**, 192 (1980).
[13] K. Danzmann, M. S. Fee, and S. Chu, Phys. Rev. A **39**, 6072 (1989).
[14] M. S. Fee, K. Danzmann, and S. Chu, Phys. Rev. A **45**, 4911 (1992).
[15] S. Gangopadhyay, N. Melikechi, and E. E. Eyler, J. Opt. Soc. Am. B **11**, 2314 (1994).
[16] N. Melikechi, S. Gangopadhyay, and E. E. Eyler, J. Opt. Soc. Am. B **11**, 2402 (1994).
[17] I. Reinhard, M. Gabrysch, B. F. von Weikersthal, K. Jungmann, and G. Z. Putlitz, Appl. Phys. B: Lasers Opt. **B63**, 467 (1996).
[18] K. S. E. Eikema, W. Ubachs, W. Vassen, and W. Hogervorst, Phys. Rev. A **55**, 1866 (1997).
[19] P. Bakule, P. E. G. Baird, M. G. Boshier, S. L. Cornish, D. F. Heller, K. Jungmann, I. C. Lane, V. Meyer, P. H. G. Sandars, W. T. Toner, M. Towrie, and J. C. Walling, Appl. Phys. B: Lasers Opt. **B71**, 11 (2000).
[20] R. T. White, Y. He, B. J. Orr, M. Kono, and K. G. H. Baldwin, J. Opt. Soc. Am. B **21**, 1577 (2004).
[21] R. T. White, Y. He, B. J. Orr, M. Kono, and K. G. H. Baldwin, Opt. Express **23**, 5655 (2004).
[22] T. W. Hänsch and B. Couillaud, Opt. Commun. **35**, 441 (1980).
[23] Y. K. Park, G. Guiliani, and R. L. Byer, IEEE J. Quantum Electron. **QE-20**, 117 (1984).
[24] J.-L. Lachambre, P. Lavigne, G. Otis, and M. Noël, IEEE J. Quantum Electron. **QE-12**, 756 (1976).
[25] M. S. Bowers and S. E. Moody, J. Opt. Soc. Am. B **11**, 2266 (1994).
[26] K. F. Wall, R. L. Aggarwal, M. D. Sciacca, H. J. Zeiger, R. E. Fahey, and A. J. Strauss, Opt. Lett. **14**, 180 (1989).
[27] S. Hannemann, Ph.D. thesis, Vrije Universiteit Amsterdam, 2007 (www.ubvu.vu.nl/dissertations/getpdf.cfm?promid=7954).
[28] D. W. Chandler and L. R. Thorne, J. Chem. Phys. **85**, 1733 (1986).
[29] R. T. White, Y. He, B. J. Orr, M. Kono, and K. G. H. Baldwin, Opt. Lett. **28**, 1248 (2003).
[30] S. Hannemann, E. Salumbides, S. Witte, R. Th. Zinkstok, K. S. E. Eikema, and W. Ubachs, Phys. Rev. A **74**, 062514 (2006).
[31] S. Hannemann, E. J. Salumbides, and W. Ubachs, Opt. Lett. **32**, 1381 (2007).
[32] S. Hannemann, E. Salumbides, S. Witte, R. Th. Zinkstok, K. S. E. Eikema, and W. Ubachs, Phys. Rev. A **74**, 012505 (2006).
[33] E. Salumbides, S. Hannemann, K. S. E. Eikema, and W. Ubachs, Mon. Not. R. Astron. Soc. **373**, L41 (2006).
[34] S. Hannemann, U. Hollenstein, E.-J. van Duijn, and W. Ubachs, Opt. Lett. **30**, 1494 (2005).
[35] M. Sneep, S. Hannemann, E.-J. van Duijn, and W. Ubachs, Opt. Lett. **29**, 1378 (2004).
[36] S. Hannemann, G. R. Wu, E.-J. van Duijn, W. Ubachs, and Ph. Cosby, J. Chem. Phys. **123**, 174318 (2005).